nature genetics

Loss of Fat4 disrupts PCP signaling and oriented cell division and leads to cystic kidney disease

Sakura Saburi[1], Ian Hester[1], Evelyne Fischer[2], Marco Pontoglio[2], Vera Eremina[1], Manfred Gessler[3], Sue E Quaggin[1,4], Robert Harrison[5], Richard Mount[5] & Helen McNeill[1,6]

Tissue organization in *Drosophila* is regulated by the core planar cell polarity (PCP) proteins Frizzled, Dishevelled, Prickle, Van Gogh and Flamingo. Core PCP proteins are conserved in mammals and function in mammalian tissue organization. Recent studies have identified another group of *Drosophila* PCP proteins, consisting of the protocadherins Fat and Dachsous (Ds) and the transmembrane protein Four-jointed (Fj). In *Drosophila*, Fat represses *fj* transcription, and Ds represses Fat activity in PCP. Here we show that *Fat4* is an essential gene that has a key role in vertebrate PCP. Loss of *Fat4* disrupts oriented cell divisions and tubule elongation during kidney development, leading to cystic kidney disease. *Fat4* genetically interacts with the PCP genes *Vangl2* and *Fjx1* in cyst formation. In addition, *Fat4* represses *Fjx1* expression, indicating that Fat signaling is conserved. Together, these data suggest that *Fat4* regulates vertebrate PCP and that loss of PCP signaling may underlie some cystic diseases in humans.

Understanding how cells develop and coordinate their polarity is essential for understanding normal development and diseases caused by defective tissue organization. A pathway controlling tissue organization, known as the planar cell polarity (PCP) pathway, was first delineated in *Drosophila melanogaster*[1,2]. Core PCP proteins[3,4] and tissue-specific effectors[5] are conserved from flies to mammals, and loss of core genes involved in vertebrate PCP results in defects in tissue organization. Recent studies have identified another group of PCP proteins in *Drosophila*, consisting of the protocadherins Fat and Dachsous (Ds) and the transmembrane protein Four-jointed (Fj)[6–9]. Fat is a large transmembrane protein, with 34 cadherin repeats, EGF and laminin domains and a conserved cytoplasmic domain (**Supplementary Fig. 1** online). Fat functions as a receptor for Ds in PCP signaling and represses transcription of *fj*[2,9–13]. Current models for *Drosophila* PCP propose that Fat and Ds function upstream of Frizzled in PCP signaling[9,14], although some studies suggest that Fat and Ds instead function in parallel to Frizzled PCP signaling[15]. In vertebrates, there are four Fat homologs (Fat1–4), two Ds homologs (Ds1 and Ds2) and one Fj ortholog (Fjx1)[16]. Fat4 alone bears extensive similarity to Fat in the intracellular, PCP signaling domain (**Supplementary Fig. 1**)[12]. This structural conservation suggests that Fat4 may function in vertebrate PCP signaling.

To test whether the Fat-Ds-Fj cassette regulates PCP in mice, we generated a null allele for *Fat4* by deleting exon 3 (**Fig. 1a–d**). Loss of *Fat4* leads to death at birth, with pups being runted, with a curved body axis and curly tails (**Fig. 1e–g** and **Supplementary Table 1** online). Mutations in vertebrate core PCP genes disrupt inner ear hair cell organization[3,4,17,18]. Scanning electron microscopy of the inner ear of *Fat4* mutants revealed subtle but statistically significant disruptions in orientation of hair cells in all levels of the cochlea (**Fig. 2a–c**; $P < 0.003$). Mutation of vertebrate core PCP genes also leads to defects in elongation of the cochlea[19]. Elongation of the cochlea is also disrupted in *Fat4* mutants, resulting in a short and broadened tissue (**Fig. 2d–g**; $P < 0.04$). Despite the smaller overall size of *Fat4* mutants, the neural tube was significantly broader than in wild-type siblings (**Fig. 2h–j**; $P < 0.007$), suggesting underlying defects in neural tube elongation. Together, these data suggest that *Fat4* regulates vertebrate PCP.

Fat4$^{-/-}$ kidneys are significantly smaller than those of wild-type siblings (**Fig. 1f,g**). Notably, histological analysis of *Fat4* mutant kidneys revealed cystic dilations of tubules and occasionally Bowman's capsule (**Fig. 3a,b**). Cystic dilations were visible as early as embryonic day 16 (E16) and increased in severity during development (**Fig. 3c,d** and data not shown). To determine whether the cystic defects in *Fat4* mutant kidneys were associated with changes in cell fate, we analyzed the expression of genes involved in kidney development. No significant changes in the expression levels of *Gpd1*, *Ret*, *Wt1*, *Dchs1*, *Wnt11*, *Wnt7b* or *Wnt9b* occurred in *Fat4*$^{-/-}$ kidneys (**Fig. 3e–h**, **Supplementary Fig. 2** online and data not shown). We conclude that *Fat4* controls tissue organization but not general cell fate determination in the kidney, consistent with the role of PCP genes in *Drosophila*.

It has been suggested that the dilated tubules associated with cystic kidney disease are due to defects in tubule elongation. To ascertain whether loss of *Fat4* leads to defects in elongation of ureteric

[1]Samuel Lunenfeld Research Institute, Mt. Sinai Hospital, Toronto M5G 1X5, Canada. [2]'Gene Expression Development and Disease' Laboratory, Developmental Biology Department, Centre National de la Recherche Scientifique URA 2578, Pasteur Institute, Paris, France. [3]Theodor-Boveri-Institute of the University of Wuerzburg, Wuerzburg D-97074, Germany. [4]St. Michael's Hospital, Toronto M5G 1X5, Canada. [5]Hospital for Sick Children, Toronto M5G 1X8, Canada. [6]Department of Molecular Genetics, University of Toronto, Toronto M5G 1X5, Canada. Correspondence should be addressed to H.M. (mcneill@mshri.on.ca).

Received 19 March; accepted 16 May; published online 6 July 2008; doi:10.1038/ng.179

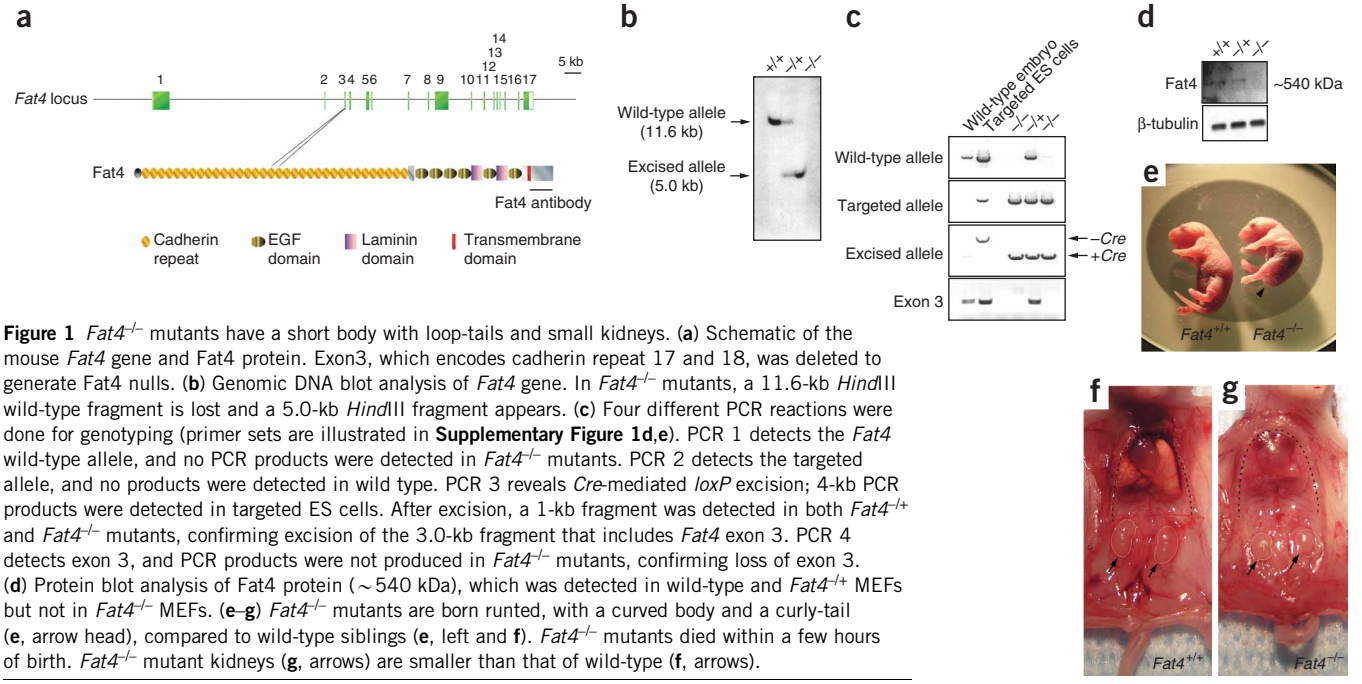

Figure 1 *Fat4*$^{-/-}$ mutants have a short body with loop-tails and small kidneys. (**a**) Schematic of the mouse *Fat4* gene and Fat4 protein. Exon3, which encodes cadherin repeat 17 and 18, was deleted to generate Fat4 nulls. (**b**) Genomic DNA blot analysis of *Fat4* gene. In *Fat4*$^{-/-}$ mutants, a 11.6-kb *Hind*III wild-type fragment is lost and a 5.0-kb *Hind*III fragment appears. (**c**) Four different PCR reactions were done for genotyping (primer sets are illustrated in **Supplementary Figure 1d**,**e**). PCR 1 detects the *Fat4* wild-type allele, and no PCR products were detected in *Fat4*$^{-/-}$ mutants. PCR 2 detects the targeted allele, and no products were detected in wild type. PCR 3 reveals *Cre*-mediated *loxP* excision; 4-kb PCR products were detected in targeted ES cells. After excision, a 1-kb fragment was detected in both *Fat4*$^{-/+}$ and *Fat4*$^{-/-}$ mutants, confirming excision of the 3.0-kb fragment that includes *Fat4* exon 3. PCR 4 detects exon 3, and PCR products were not produced in *Fat4*$^{-/-}$ mutants, confirming loss of exon 3. (**d**) Protein blot analysis of Fat4 protein (~540 kDa), which was detected in wild-type and *Fat4*$^{-/+}$ MEFs but not in *Fat4*$^{-/-}$ MEFs. (**e**–**g**) *Fat4*$^{-/-}$ mutants are born runted, with a curved body and a curly-tail (**e**, arrow head), compared to wild-type siblings (**e**, left and **f**). *Fat4*$^{-/-}$ mutants died within a few hours of birth. *Fat4*$^{-/-}$ mutant kidneys (**g**, arrows) are smaller than that of wild-type (**f**, arrows).

bud-derived tubular structures, we stained wild-type and *Fat4*$^{-/-}$ kidneys with the lectin DBA and observed a generalized loss of elongated tubules in *Fat4*$^{-/-}$ kidneys (**Supplementary Fig. 3** online). Aquaporin 2 (Aqp2)-positive collecting ducts were short and broad in *Fat4* mutants and did not form extended tubular structures (**Fig. 4a–d**). Similarly, staining with antibodies to Tamm Horsfall protein (THP), which marks the Loop of Henle, revealed reduced and broadened tubules (**Fig. 4e–h**) in *Fat4* mutants. There were no significant changes in proliferation or apoptosis in *Fat4* mutant kidneys at E16.5 (**Supplementary Fig. 4** online and data not shown). Thus, cysts are likely due not to inappropriate cell numbers, but instead to defective elongation of kidney tubules.

PCP has been implicated in the control of oriented cell division (OCD)[1,2,19,20]. OCD contributes to the normal elongation of kidney tubules during development, and cystic dilations can be caused by a loss of OCD[21]. To determine whether the defects seen in *Fat4* mutant kidneys could be due to loss of OCD, we measured the mitotic angle of *Fat4* mutant tubule epithelial cells. The mitotic angle is defined as the difference in orientation between mitotic separating chromosomes and the tubule axis during anaphase or telophase. We used an antibody to H3pS10 to label mitotic chromosomes and determined the orientation of the tubule axis using antibodies to Aqp2 or the lectin *Lotus tetragonolobus*. In newborn kidneys, mitotic angles are tightly controlled, with 80% of mitotic angles less than 30° off the tubule axis (**Fig. 4i**,**j**). In contrast, in *Fat4*$^{-/-}$ kidneys, the tight control of OCD is lost (Mann-Whitney U test; $P < 0.014$; **Fig. 4i**,**j**). Notably, in *Drosophila*, loss or gain of the Fat ligand Ds, or overexpression of Fat, also leads to loss of OCD, resulting in wing elongation defects[20]. Therefore, the role of Fat-like cadherins in OCD and tissue elongation is conserved.

Drosophila fat represses transcription of *fj*[9]. To further probe conservation of the Fat-Ds-Fj signaling pathway, we analyzed the expression of the vertebrate ortholog of *fj*, *Fjx1*, in *Fat4* mutants. *In situ* hybridization analysis revealed that *Fjx1* is upregulated in *Fat4*$^{-/-}$ kidneys from newborn mice (**Fig. 4k**,**l**), as well as at E16.5 (**Supplementary Fig. 5** online). *Fjx1* upregulation was marked in the tubules, where *Fjx1* is normally expressed; however, we also frequently noted upregulation in surrounding tissues (data not shown). In *Drosophila*, *fj* can non-autonomously induce its own transcription[6]; thus, the increased expression of *Fjx1* in tubules may lead to increased expression seen in surrounding nontubular tissues in *Fat4* mutants. Therefore, the role of Fat in the control of the PCP protein Fj is conserved.

To test whether the cystic phenotype of *Fat4* mutants is affected by loss of core PCP genes, we generated mice that had lost one copy of the PCP gene *Vangl2* in a *Fat4*-homozygous mutant background (**Fig. 5**). Loss of one copy of *Vangl2* led to occasional, minor dilations in tubules that were not statistically significant (**Fig. 5b**,**e**). In contrast, we observed a marked increase in the severity of cystic tubules in *Fat4* mutants when one copy of *Vangl2* was mutated ($P < 0.05$; **Fig. 5d**,**e**). This suggests that *Fat4* acts in a partially redundant fashion with *Vangl2* during cyst formation.

To determine whether *Fjx1* regulation by *Fat4* has a role in cystic kidney disease, we first examined mice mutant for *Fjx1*. Mice null for *Fjx1* are viable and fertile, with no reported defects in kidney function[22]. Our histological analysis of the kidneys of *Fjx1*-null mice revealed no significant defects in kidney organization (**Supplementary Fig. 5**). This is similar to *Drosophila*, where loss of *fj* has no effect on viability and leads to only very subtle defects in PCP (~0.3% defects in PCP in the fly eye[6]). To determine whether the increased expression of *Fjx1* in *Fat4* mutants was relevant to the development of cysts, we examined the effects of simultaneous loss of *Fat4* and *Fjx1*. Notably, loss of *Fat4* and *Fjx1* leads to enhancement of the cystic defects seen in *Fat4*-mutant kidneys (**Fig. 5f**,**g** and **Supplementary Fig. 5**). Cystic dilations are obvious by E16.5 (**Supplementary Fig. 5**). These dilations were so extreme that they occasionally resulted in dramatically enlarged kidneys. These enlarged kidneys were associated with hydronephrosis and doubled ureters and the appearance of duplex kidneys (**Fig. 5f**,**g**), similar to those seen in *Foxc1* mutants[23]. These phenotypes were never seen in *Fat4*-homozygous mutants, suggesting

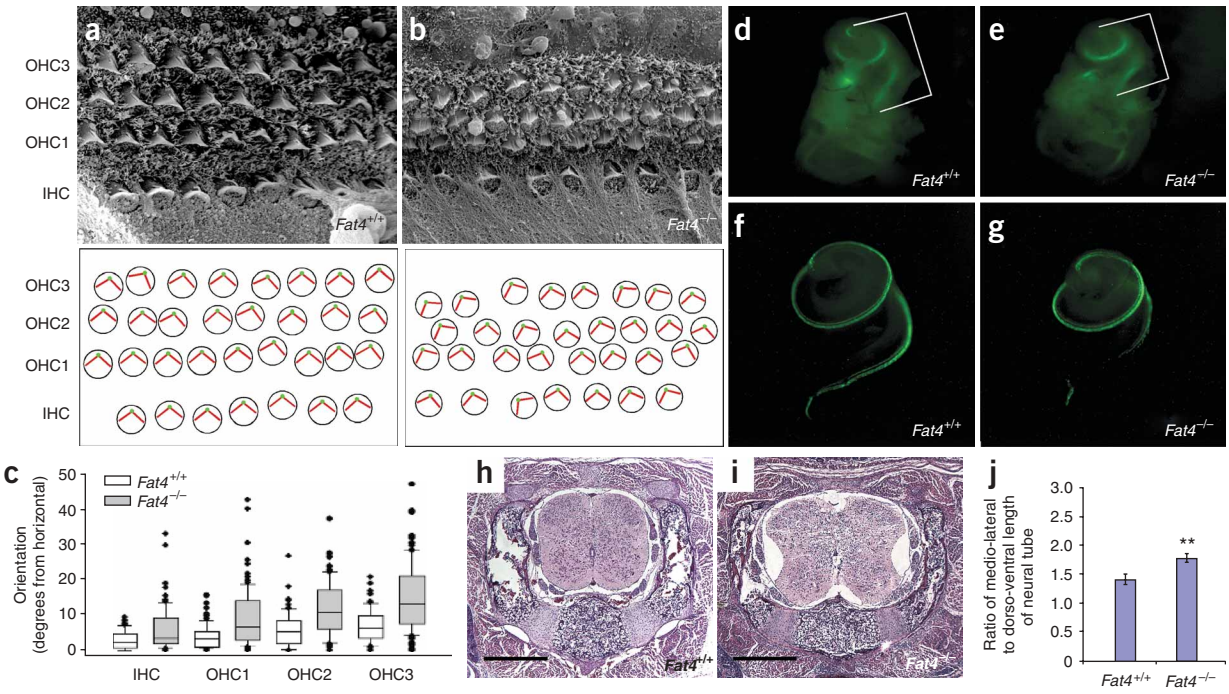

Figure 2 Loss of Fat4 leads to PCP defects. (**a**,**b**) Scanning electron microscopic analysis of middle turn of the organ of Corti in P0 wild-type (**a**) and *Fat4*$^{-/-}$ mutants (**b**). In *Fat4*$^{-/-}$ mutants, hair cells are misorientated throughout the cochlea. (**c**) Statistical analysis of hair cell orientation, measured as degrees of deviation from the horizontal axis of the organ of Corti. *Fat4*$^{-/-}$ mutants showed significantly more deviations than wild-type siblings in all turns of the cochlea and in all rows of hair cells. Statistical analysis by Mann-Whitney rank sum test ($P < 0.003$ for IHC; $P < 0.001$ for OHC1–3). Statistical analysis by a two-tail *t*-test ($P = 0.0003$ for IHC, $P < 4.0 \times 10^{-8}$ for OHC1–3). (**d**,**e**) Inner ears dissected from P0 wild-type (**d**) and *Fat4*$^{-/-}$ mutants (**e**). The cochlear duct (brackets) was consistently smaller than the vestibule in *Fat4*$^{-/-}$ mutants compared to wild-type siblings ($P < 0.04$). (**f**,**g**) Dissected organ of Corti from newborn wild-type (**f**) and *Fat4*$^{-/-}$ (**g**) mutant cochlear ducts. Mechanosensory hair cells were visualized by green fluorescent protein (GFP) driven by hair cell–specific promoter Math-1. The organ of Corti was shorter in *Fat4*$^{-/-}$ mutants than in wild-type siblings, suggesting defective tissue elongation. (**h**,**i**) Despite the smaller size of *Fat4*$^{-/-}$ mutants, the neural tube (**i**) was significantly wider in mutants than in wild-type siblings (**h**). Scale bar, 500 μm. (**j**) Statistical analysis of width of neural tube. The diameter of neural tube was measured along both medio-lateral and dorso-ventral axis. Error bars, s.d. $^{**}P < 0.007$.

that *Fjx1* may also affect *Fat4*-independent pathways in kidney development. The biochemical function of Fjx1 is unclear; however, it is thought that Fj may modify Fat or Ds to regulate PCP signaling. Thus, the synergistic effects of loss of *Fat4* and *Fjx1* in cyst formation may be due to loss of Fjx1 modulation of the other Fat-like cadherins (Fat1–3) or of Dchs1 or Dchs2. The relatively subtle defects in inner ear hair cell orientation in *Fat4* mutants may also be a result of redundancy with the other *Fat* genes. Loss of *Fat1* has no effect on

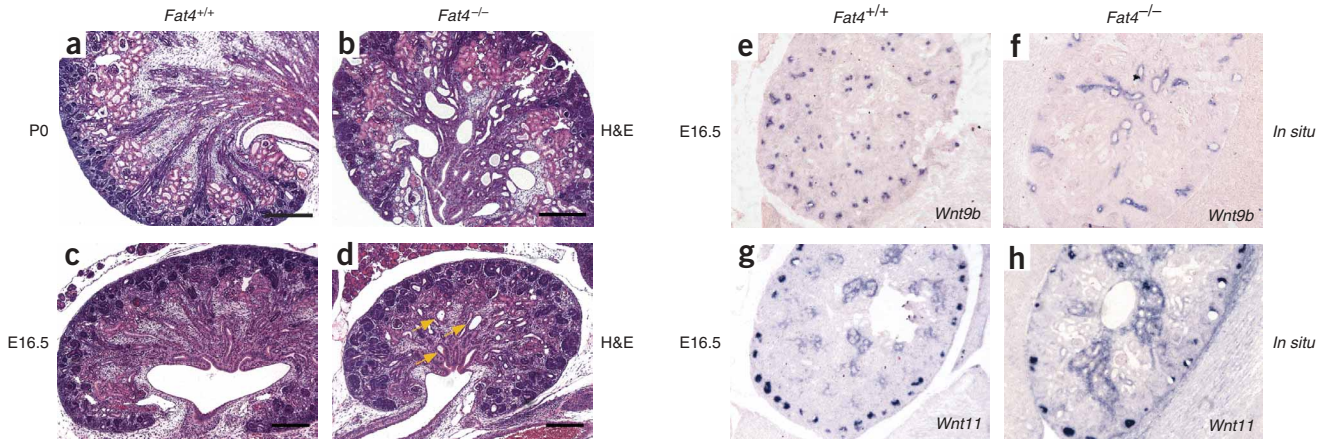

Figure 3 Loss of Fat4 results in cystic kidney disease. (**a**,**b**) Histological analysis of P0 wild-type (**a**) and *Fat4*$^{-/-}$ mutant kidneys (**b**). *Fat4* mutants developed cystic dilations of renal tubules and expansion of intraglomerular space of the nephrons. Scale bar, 500 μm. (**c**,**d**) Histological analysis of E16.5 wild-type (**c**) and *Fat4*$^{-/-}$ homozygous mutant kidneys (**d**). Some renal tubules are cystic at E16.5 in *Fat4*$^{-/-}$ homozygous mutant kidneys. Scale bar, 200 μm. (**e**–**h**) *In situ* hybridization analysis of E16.5 wild-type and *Fat4*$^{-/-}$ homozygous mutant kidneys with *Wnt9b*- (**e**,**f**) and *Wnt11*-specific (**g**,**h**) riboprobes. No significant changes were detected in *Fat4*$^{-/-}$ homozygous mutant kidneys.

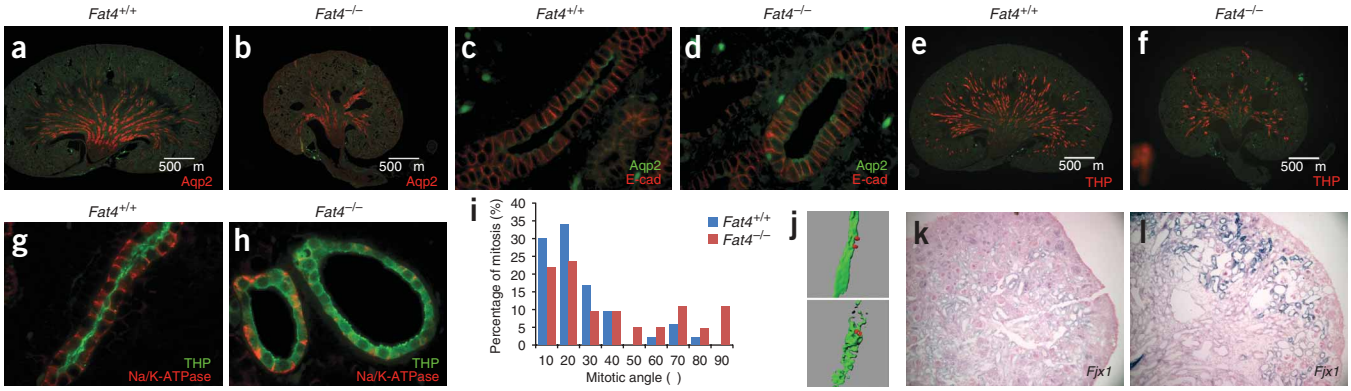

Figure 4 Defects in PCP signaling, oriented cell division and tubule elongation in *Fat4* mutant kidneys. (**a**,**b**) Immunofluorescence with a marker of collecting duct, Aquaporin2 (Aqp2) antibody on P0 wild-type (**a**) and *Fat4*$^{-/-}$ mutant kidneys (**b**). Aqp2-positive tubular segments were short and broadened in *Fat4*$^{-/-}$ mutants. (**c**,**d**) Aqp2 (green) and E-cadherin (red) staining of E16.5 wild-type (**c**) and *Fat4*$^{-/-}$ mutants (**d**) illustrating at high power the dilation of tubules in *Fat4*$^{-/-}$ mutants. (**e**,**f**) Dilation of Henle's loop, visualized with antibodies to Tamm Horsfall protein (THP), in *Fat4*$^{-/-}$ mutant kidneys (**f**) compared to those of wild-type siblings (**e**). THP-positive tubular segments were frequently shorter and broader than in wild type. (**g**,**h**) Dilation of Henle's loop visualized with anti-THP (green) and Na^+/K^+-ATPase (red) in E17.5 *Fat4*$^{-/-}$ mutants (**h**) compared to wild-type siblings (**g**). (**i**,**j**) Oriented cell division is disrupted in *Fat4*$^{-/-}$ mutants. Mitotic angles were determined and the incidence of each angle is plotted for wild-type and *Fat4*$^{-/-}$ mutants in P0 newborn kidneys. There is a significant difference in the distribution of wild-type and *Fat4*$^{-/-}$ mutant mitotic angles ($P = 0.0146$: Kolmogorov-Smirnov test: 51 mutant mitoses, 53 wild-type mitoses). Examples of Normal axis of division in wild-type (top) and defective OCD (bottom) from *Fat4*$^{-/-}$ tubules (**j**). (**k**,**l**) *Fjx1* expression increases in *Fat4*$^{-/-}$ mutants. *Fjx1* transcripts were weakly detected in wild-type kidneys (**k**). In *Fat4*$^{-/-}$ mutant kidneys (**l**), strong expression of *Fjx1* transcripts was observed in a subset of renal tubules.

vertebrate PCP[24], but the other *Fat*-like genes (*Fat2* and *Fat3*) have not yet been genetically ablated; thus, their function in vertebrate PCP is still unknown.

The Fat-Ds-Fj cassette has generally been accepted to act upstream of the core PCP genes[2,10,14]; however, a recent study raised the possibility that they may act in parallel pathways in *Drosophila*[15]. Additional support for this hypothesis comes from our observation of strong genetic interactions between *Fat4* and *Vangl2* (**Fig. 5a–e**) in cyst formation, suggesting that they act in parallel pathways. There are also significant genetic interactions between *Fat4* and *Vangl2* in viability (**Supplementary Table 2** online). Loss of *Fat4* does not affect the distribution of Vangl2 (**Fig. 5h–k**) or Fz6 (data not shown), which is also consistent with a parallel pathway model.

To explore the subcellular localization of Fat4, we turned to MDCK cells, which are highly polarized kidney epithelial cells. We found that Fat4 is localized to primary cilia in MDCK cells (**Supplementary Fig. 6** online). To determine whether Fat4 is needed for formation of primary cilia, we examined cilia with antibodies to acetylated tubulin

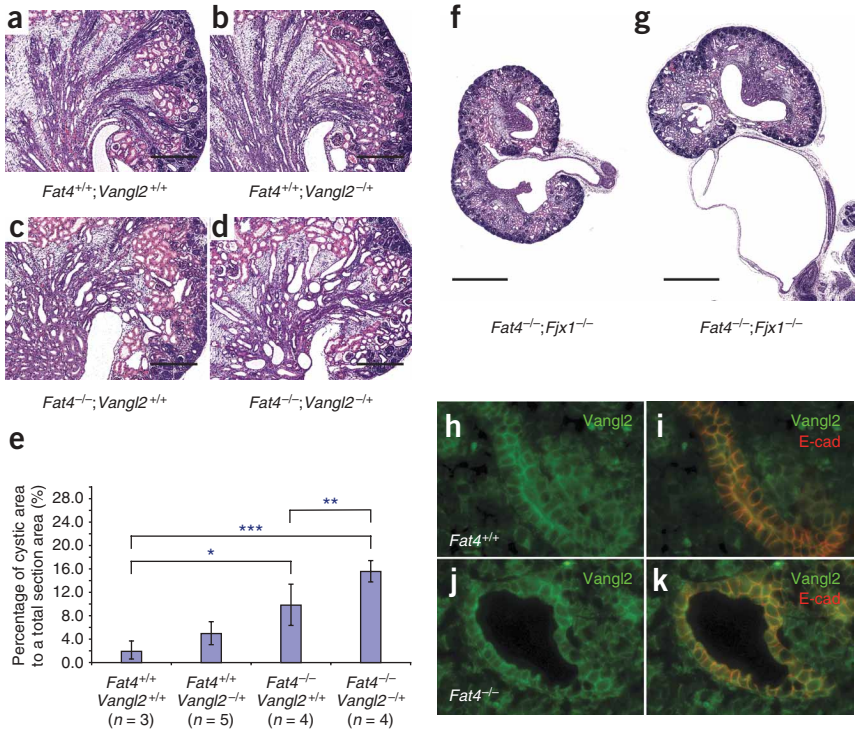

Figure 5 Genetic interaction of *Fat4* with *Vangl2* and *Fjx1* in cyst formation. (**a**–**d**) Loss of one copy of *Vangl2* markedly enhances cyst formation in *Fat4*$^{-/-}$ mutants. (**a**) Wild-type kidney. (**b**) Loss of one copy of *Vangl2* does not result in obvious cysts. (**c**) *Fat4*$^{-/-}$ mutants have consistent cysts that are enhanced in *Fat4*$^{-/-}$;*Vangl2*$^{-/+}$ mutants (**d**). Scale bar, 500 μm. (**e**) Morphometric analysis of kidneys shows that the enhancement of cysts in P0 *Fat4*$^{-/-}$ mutants by loss of one copy of *Vangl2* is statistically significant, whereas loss of one copy of *Vangl2* does not significantly enhance cyst formation in otherwise wild-type animals. $^*P < 0.02$, $^{**}P < 0.007$, $^{***}P < 0.0002$. Error bars, s.d. (**f**,**g**) Loss of *Fjx1* enhances the cystic defects of *Fat4*$^{-/-}$ homozygous mutants. Histological analysis of *Fat4*$^{-/-}$;*Fjx1*$^{-/-}$ double mutant kidneys shows more cystic tubules and a dilated intraglomerular space. Occasionally, massive cysts were seen in this genotype, as well as hydronephrosis and a doubled ureter. Scale bar, 1 mm. (**h**–**k**) The expression pattern of Vangl2 was not altered in E15.5 *Fat4*$^{-/-}$ kidneys. (**h**,**i**) In wild-type kidneys, Vangl2 (green) is localized to basolateral and apical membranes. Co-staining with antibodies to E-cadherin (red) marks lateral membranes. (**j**,**k**) No changes in Vangl2 distribution could be detected in *Fat4*$^{-/-}$ mutant kidneys.

in *Fat4*$^{-/-}$ kidneys. We did not detect any alterations in cilia number by confocal microscopy in most *Fat4*$^{-/-}$ tubules; however, we did occasionally see reduced cilia in larger cystic structures (**Supplementary Fig. 6**). PC1 and PC2, which are altered in human autosomal dominant polycystic kidney disease, are also localized to primary cilia. Loss of PC1 or PC2 does not affect cilia formation but does affect the ability of the primary cilium to function as a flow sensor[25]. Mutations in genes encoding a number of cilia-associated proteins result in cystic diseases in humans[26,27], and loss of cilia can lead to cyst formation in mice[28]. Thus, the localization of Fat4 to primary cilia supports the hypothesis that the cilium is a key organelle for PCP signaling[5] and that cystic kidney disease is linked to defective PCP signaling.

Loss of *Fat4* leads to defects in polarity of hair cells of the inner ear as well as defects in tissue elongation in the cochlea and the neural tube. These are classic PCP phenotypes, supporting the proposal that *Fat4* functions to regulate PCP in vertebrates. Significantly, *Fat4* represses *Fjx1* transcription in mice, much as *fat* represses *fj* transcription in *Drosophila*, indicating that the PCP signaling pathway is conserved. In *Drosophila*, disrupting Fat signaling causes wing elongation defects during development[20]. Loss of *Fat4* also leads to defects in OCD in the developing kidney, indicating that the control of OCD is a conserved function of the Fat family of cadherins and providing a mechanism for the tubular dilations and cysts observed in *Fat4* mutants.

Together, these results demonstrate that the Fat-Ds-Fj PCP signaling cassette is conserved in vertebrates and provide experimental evidence to support the hypothesis that polycystic kidney disease can be caused by defective PCP signaling. Polycystic kidney disease is a devastating condition, with severe social and economic consequences[29]. It has been speculated that cystic kidney disease might be due to defective PCP[21,30]. Our studies provide the first experimental support for this hypothesis and establish a mammalian model of cystic kidney disease caused by defective PCP.

METHODS

Generation of a *Fat4* loss-of-function allele. Mouse *Fat4* genomic DNA was isolated from a RPCI-22 PAC library (Invitrogen) of 129S6/SvEvTAC (CHORI) mouse genomic DNA. The *Fat4* conditional targeting vector was constructed using pFlrt (a gift from I. Rosewell, Cancer Research UK) as a backbone vector. The *Fat4* conditional targeting vector (**Supplementary Fig. 1**) was introduced into mouse embryonic stem (ES) cells, 129/1 (129P2/Ola strain, Cancer Research UK), by electroporation, and G418 resistant clones were screened by PCR and genomic Southern blot analysis. *Fat4* germ-line chimeras were generated by blastocyst injection of homologous recombinant ES cells. *Fat4* germ-line chimeras were crossed to *Ella-Cre* mice (FVB/N-Tg(*Ella-Cre*); The Jackson Laboratory) to remove exon 3, producing a *Fat4*-null allele. *Fat4*$^{-/+}$ mice were sib crossed to produce *Fat4*-null mice analyzed in these studies (referred to as *Fat4*$^{\Delta flox/\Delta flox}$ or *Fat4*$^{-/-}$).

Protein blot analysis. Proteins extracts were prepared from E14.5 mouse embryonic fibroblasts (MEFs) by boiling for 3 min in sample buffer. Fifteen micrograms of each protein extract was loaded on 3–8% NuPage gradient tris-acetate (TA) acrylamide gel (BioRad) and blotted overnight onto immune-Blot PVDF membrane (BioRad). Membranes were probed with rat Fat4-Ic antibody. Visualization was achieved by chemiluminescence (ECL-Plus GE Healthcare).

Histological analysis. Embryos were dissected from *Fat4*$^{-/+}$ females, crossed to *Fat4*$^{-/+}$ males, at specific embryonic stages and fixed with 10% formaldehyde overnight. We processed the fixed embryos and kidneys for paraffin embedding using standard procedures. Sections were cut at a thickness of 4 μm with a microtome and placed on poly-L-lysine–coated slides. After drying at 60 °C for 2 h, sections were stained with hematoxylin and eosin.

***In situ* hybridization.** Embryos were dissected from *Fat4*$^{-/+}$ females, crossed to *Fat4*$^{-/+}$ males, at specific embryonic stages (E16.5 and P0), and fixed with 4% PFA in PBS at 4 °C overnight. We dissected P0 kidneys from newborn wild-type and various mutants and fixed as described above. Fixed embryos and kidneys were washed with PBS and treated with 15% sucrose in PBS at 4 °C overnight, followed by 30% sucrose at 4 °C overnight. Embryos were embedded into OCT compound in liquid nitrogen and sectioned at a thickness of 6 μm. We prepared digoxigenin (DIG)-labeled RNA probes using a linearized plasmid DNA. Additional details are provided in **Supplementary Methods** online.

Immunofluorescence. We sectioned frozen embryos and kidneys to 16 μm and 10 μm thickness, respectively. Sections were washed for a 15 min in PBS and then immersed in 0.01M sodium citrate (pH 6.0) at 95 °C for 20 min. The solution was cooled at room temperature for 20 min, washed in PBS and then processed. Additional details are provided in **Supplementary Methods**.

Scanning electron microscopic analysis of the organ of Corti. We dissected the inner ears from newborn wild-type and *Fat4*$^{-/-}$ mutants in cold PBS and fixed them at room temperature for 2 h in 2.5% glutaraldehyde in 0.1M sodium cacodylate buffer. The organ of Corti was processed for scanning electron microscope analysis as described in the **Supplementary Methods**. We photographed the organ of Corti at ×2500 magnification, excluding the apical-most and basal-most half-turns. The field of view included 10–12 outer hair cells from each row. For analysis, we oriented photomicrographs such that a line through the central eight OHC2s (outer hair cell row 2) was horizontal. We marked the orientation of each stereocilia bundle and measured its absolute deviation from the horizontal measured using ImageJ 1.37v software (see URLs section below).

Mitotic spindle orientation analysis. We carried out indirect immunofluorescence on vibratome sections to determine spindle orientation. Kidneys were fixed in 4% formaldehyde for 30 min, washed in PBS and embedded in 4% agarose. We incubated 100-μm vibrotome sections with primary antibodies (anti-Aquaporin2 biotinylated (Nato), anti-H3pS10 and biotinylated Lotus Tetragonolobus Lectin (LTL, AbCys Biology)) in PBS, 10% FCS, 0.1% Triton X-100 overnight at 4 °C. Sections were rinsed several times in PBS and incubated with secondary antibody (FITC conjugated streptavidin and Texas red–linked anti-rabbit IgG) in PBS with 10% FCS, Triton X-100 0.1% overnight at 4 °C. After 24 h washing in PBS, sections were mounted on slides with Vectashield medium and covered by a coverslip. We collected and analyzed images as previously described[21]. See **Supplementary Methods** for more details.

Quantitative analysis of cystogenesis. P0 kidneys from newborn pups were processed for hematoxylin and eosin. We digitized the entire slide with Aperio Scanner (Aperio ScanScope XT; Aperio Technologies) and quantifed the images for cystic area with morphometric imaging software (Image-Pro; Media Cybernetics). We set the lower threshold as 200 μm^2 to identify dilated luminal area. All sets of cystic area were summed, and the area was divided by total section area.

URLs. ImageJ 1.37v software, http://rsb.info.nih.gov/ij/.

Note: Supplementary information is available on the Nature Genetics website.

ACKNOWLEDGMENTS

We are grateful to I. Rosewell of Cancer Research UK for help in generating the *Fat4* germline chimeras. We also thank J. Hoyer (University of Delaware), M. Knepper (National Heart, Lung, and Blood Institute), T. Carroll (University of Texas Southwestern), B. Bruneau (University of California, San Francisco) and the Developmental Studies Hybridoma bank for antibodies and probes, J. Johnson (University of Texas Southwestern) for the Math-1-GFP mice, P. Gros (McGill University) for mice and antibodies and A. Vortkamp (Universitaet Duisburg-Essen) for help with generating the *Fjx1*-null mice. This work was supported by grants from the Canadian Institute for Health Research (MOP84468) and Cancer Research UK to H.M. and from the Fondation pour la Recherche Medical and PKD foundation to M.P. We apologize to those whose work we were unable to cite because of space constraints.

AUTHOR CONTRIBUTIONS

S.S. and H.M. designed the experiments, analyzed the data and wrote the paper. M.G. provided mice. R.M. and R.H. analyzed the inner ear phenotype. S.S., V.E. and I.H. conducted the *in situ* hybridizations. E.F. and M.P. analyzed

spindle orientation. S.S. analyzed the cochlea elongation phenotype, neural tube phenotype and cystic kidney morphometric analysis. S.E.Q. helped in the analysis of cystic kidney phenotypes. S.S. and I.H. conducted the immunohistochemistry.

Published online at http://www.nature.com/naturegenetics/
Reprints and permissions information is available online at http://npg.nature.com/reprintsandpermissions/

1. Seifert, J.R. & Mlodzik, M. Frizzled/PCP signalling: a conserved mechanism regulating cell polarity and directed motility. *Nat. Rev. Genet.* **8**, 126–138 (2007).
2. Saburi, S. & McNeill, H. Organising cells into tissues: new roles for cell adhesion molecules in planar cell polarity. *Curr. Opin. Cell Biol.* **17**, 482–488 (2005).
3. Montcouquiol, M. *et al.* Identification of *Vangl2* and *Scrb1* as planar polarity genes in mammals. *Nature* **423**, 173–177 (2003).
4. Curtin, J.A. *et al.* Mutation of *Celsr1* disrupts planar polarity of inner ear hair cells and causes severe neural tube defects in the mouse. *Curr. Biol.* **13**, 1129–1133 (2003).
5. Park, T.J., Haigo, S.L. & Wallingford, J.B. Ciliogenesis defects in embryos lacking inturned or fuzzy function are associated with failure of planar cell polarity and Hedgehog signaling. *Nat. Genet.* **38**, 303–311 (2006).
6. Zeidler, M.P., Perrimon, N. & Strutt, D.I. The *four-jointed* gene is required in the *Drosophila* eye for ommatidial polarity specification. *Curr. Biol.* **9**, 1363–1372 (1999).
7. Casal, J., Struhl, G. & Lawrence, P.A. Developmental compartments and planar polarity in *Drosophila*. *Curr. Biol.* **12**, 1189–1198 (2002).
8. Rawls, A.S., Guinto, J.B. & Wolff, T. The cadherins fat and dachsous regulate dorsal/ventral signaling in the *Drosophila* eye. *Curr. Biol.* **12**, 1021–1026 (2002).
9. Yang, C.H., Axelrod, J.D. & Simon, M.A. Regulation of Frizzled by fat-like cadherins during planar polarity signaling in the *Drosophila* compound eye. *Cell* **108**, 675–688 (2002).
10. Fanto, M. *et al.* The tumor-suppressor and cell adhesion molecule Fat controls planar polarity via physical interactions with Atrophin, a transcriptional co-repressor. *Development* **130**, 763–774 (2003).
11. Simon, M.A. Planar cell polarity in the *Drosophila* eye is directed by graded Four-jointed and Dachsous expression. *Development* **131**, 6175–6184 (2004).
12. Matakatsu, H. & Blair, S.S. Separating the adhesive and signaling functions of the Fat and Dachsous protocadherins. *Development* **133**, 2315–2324 (2006).
13. Matakatsu, H. & Blair, S.S. Interactions between Fat and Dachsous and the regulation of planar cell polarity in the *Drosophila* wing. *Development* **131**, 3785–3794 (2004).
14. Ma, D., Yang, C.H., McNeill, H., Simon, M.A. & Axelrod, J.D. Fidelity in planar cell polarity signalling. *Nature* **421**, 543–547 (2003).
15. Casal, J., Lawrence, P.A. & Struhl, G. Two separate molecular systems, Dachsous/Fat and Starry night/Frizzled, act independently to confer planar cell polarity. *Development* **133**, 4561–4572 (2006).
16. Rock, R., Schrauth, S. & Gessler, M. Expression of mouse *dchs1, fjx1*, and *fat-j* suggests conservation of the planar cell polarity pathway identified in *Drosophila*. *Dev. Dyn.* **234**, 747–755 (2005).
17. Jones, C. & Chen, P. Planar cell polarity signaling in vertebrates. *Bioessays* **29**, 120–132 (2007).
18. Wang, Y., Guo, N. & Nathans, J. The role of Frizzled3 and Frizzled6 in neural tube closure and in the planar polarity of inner-ear sensory hair cells. *J. Neurosci.* **26**, 2147–2156 (2006).
19. Gong, Y., Mo, C. & Fraser, S.E. Planar cell polarity signalling controls cell division orientation during zebrafish gastrulation. *Nature* **430**, 689–693 (2004).
20. Baena-Lopez, L.A., Baonza, A. & Garcia-Bellido, A. The orientation of cell divisions determines the shape of *Drosophila* organs. *Curr. Biol.* **15**, 1640–1644 (2005).
21. Fischer, E. *et al.* Defective planar cell polarity in polycystic kidney disease. *Nat. Genet.* **38**, 21–23 (2006).
22. Probst, B., Rock, R., Gessler, M., Vortkamp, A. & Puschel, A.W. The rodent Four-jointed ortholog Fjx1 regulates dendrite extension. *Dev. Biol.* **312**, 461–470 (2007).
23. Kume, T., Deng, K. & Hogan, B.L. Murine forkhead/winged helix genes *Foxc1* (Mf1) and *Foxc2* (Mfh1) are required for the early organogenesis of the kidney and urinary tract. *Development* **127**, 1387–1395 (2000).
24. Ciani, L., Patel, A., Allen, N.D. & ffrench-Constant, C. Mice lacking the giant protocadherin mFAT1 exhibit renal slit junction abnormalities and a partially penetrant cyclopia and anophthalmia phenotype. *Mol. Cell. Biol.* **23**, 3575–3582 (2003).
25. Nauli, S.M. *et al.* Polycystins 1 and 2 mediate mechanosensation in the primary cilium of kidney cells. *Nat. Genet.* **33**, 129–137 (2003).
26. Yoder, B.K. Role of primary cilia in the pathogenesis of polycystic kidney disease. *J. Am. Soc. Nephrol.* **18**, 1381–1388 (2007).
27. Hildebrandt, F. & Otto, E. Cilia and centrosomes: a unifying pathogenic concept for cystic kidney disease? *Nat. Rev. Genet.* **6**, 928–940 (2005).
28. Patel, V. *et al.* Acute kidney injury and aberrant planar cell polarity induce cyst formation in mice lacking renal cilia. *Hum. Mol. Genet.* **17**, 1578–1590 (2008).
29. Torres, V.E. & Harris, P.C. Mechanisms of disease: autosomal dominant and recessive polycystic kidney diseases. *Nat. Clin. Pract. Nephrol.* **2**, 40–55 (2006).
30. Simons, M. & Walz, G. Polycystic kidney disease: cell division without a c(l)ue? *Kidney Int.* **70**, 854–864 (2006).